south-eastern Atlantic Ocean, upstream of any influence from the Agulhas Current. The Agulhas Return Current can therefore be considered to have terminated here. The continuing flow along the Subtropical Convergence east of here is known as the South Indian Ocean Current.

Conclusion

The Agulhas Current is unusual as a western boundary current for a number of reasons. First, because the African continent terminates at relatively low latitudes, the current penetrates freely into the adjacent ocean basin and a substantial leakage between basins is feasible. Second, through the process of ring and filament shedding, an interaction between a western boundary current and an extensive coastal upwelling regime is brought about that is geographically not possible elsewhere. Third, the very stable nature of the northern Agulhas Current and its characteristic Natal Pulse creates a dynamic environment in which mesoscale disturbances can have profound circulatory effects downstream. The contemporary ignorance about the East Madagascar Current, about the circulation of the Mozambique Channel, and about the origin of midocean eddies in the South West Indian Ocean needs to be eliminated. Only then will a more realistic concept of the interactions between elements of the greater Agulhas Current system become possible.

See also

Mesoscale Eddies. Ocean Circulation. Water Types and Water Masses.

Further Reading

De Ruijter WPM, Biastoch A, Drijfhout SS *et al.* (1999) Indian–Atlantic inter-ocean exchange: dynamics, estimation and impact. *Journal of Geophysical Research* 104: 20885–20911.

Lutjeharms JRE (1996) The exchange of water between the South Indian and the South Atlantic. In: Wefer G, Berger WH, Siedler G and Webb D (eds) *The South Atlantic: Present and Past Circulation*, pp. 125–162. Berlin: Springer-Verlag.

Lutjeharms JRE (2001) *The Agulhas Current*. Berlin: Springer-Verlag.

Shannon LV (1985) The Benguela Ecosystem. 1. Evolution of the Benguela, physical features and processes. *Oceanography and Marine Biology, An Annual Review* 23: 105–182.

Shannon LV and Nelson G (1996) The Benguela: large scale features and processes and system variability. In: Wefer G, Berger WH, Siedler G and Webb D (eds) *The South Atlantic: Present and Past Circulation*, pp. 163–210. Berlin: Springer-Verlag.

AIRCRAFT REMOTE SENSING

L. W. Harding, Jr and W. D. Miller, University of Maryland, College Park, MD, USA
R. N. Swift and C. W. Wright, NASA Goddard Space Flight Center, Wallops Island, VA, USA

doi:10.1006/rwos.2001.0425

Introduction

The use of aircraft for remote sensing has steadily grown since the beginnings of aviation in the early twentieth century and today there are many applications in the Earth sciences. A diverse set of remote sensing uses in oceanography developed in parallel with advances in aviation, following increased aircraft capabilities and the development of instrumentation for studying ocean properties. Aircraft improvements include a greatly expanded range of operational altitudes, development of the Global Positioning System (GPS) enabling precision navigation, increased availability of power for instruments, and longer range and duration of missions. Instrumentation developments include new sensor technologies made possible by microelectronics, small, high-speed computers, improved optics, and increased accuracy of digital conversion of electronic signals. Advances in these areas have contributed significantly to the maturation of aircraft remote sensing as an oceanographic tool.

Many different types of aircraft are currently used for remote sensing of the oceans, ranging from balloons to helicopters, and from light, single engine piston-powered airplanes to jets. The data and information collected on these platforms are commonly used to enhance sampling by traditional oceanographic methods, giving increased spatial and temporal resolution for a number of important properties. Contemporary applications of aircraft remote sensing to oceanography can be grouped

into several areas, among them ocean color, sea surface temperature (SST), sea surface salinity (SSS), wave properties, near-shore topography, and bathymetry. Prominent examples include thermal mapping using infrared (IR) sensors in both coastal and open ocean studies, lidar and visible radiometers for ocean color measurements of phytoplankton distributions and 'algal blooms', and passive microwave sensors to make observations of surface salinity structure of estuarine plumes in the coastal ocean. These topics will be discussed in more detail in subsequent sections. Other important uses of aircraft remote sensing are to test instruments slated for deployment on satellites, to calibrate and validate space-based sensors using aircraft-borne counterparts, and to make 'underflights' of satellite instruments and assess the efficacy of atmospheric corrections applied to data from space-based observations.

Aircraft have some advantages over satellites for oceanography, including the ability to gather data under cloud cover, high spatial resolution, flexibility of operations that enables rapid responses to 'events', and less influence of atmospheric effects that complicate the processing of satellite data. Aircraft remote sensing provides nearly synoptic data and information on important oceanographic properties at higher spatial resolution than can be achieved by most satellite-borne instruments. Perhaps the greatest advantage of aircraft remote sensing is the ability to provide consistent, high-resolution coverage at larger spatial scales and more frequent intervals than are practical with ships, making it feasible to use aircraft for monitoring change.

Disadvantages of aircraft remote sensing include the relatively limited spatial coverage that can be obtained compared with the global coverage available from satellite instruments, the repeated expense of deploying multiple flights, weather restrictions on operations, and lack of synopticity over large scales. Combination of the large-scale, synoptic data that are accessible from space with higher resolution aircraft surveys of specific locations is increasingly recognized as an important and useful marriage that takes advantages of the strengths of both approaches.

This article begins with a discussion of sensors that use lasers (also called active sensors), including airborne laser fluorosensors that have been used to measure chlorophyll (chl-a) and other properties; continues with discussions of lidar sensors used for topographic and bathymetric mapping; describes passive (sensors that do not transmit or illuminate, but view naturally occurring reflections and emissions) ocean color remote sensing directed at quantifying phytoplankton biomass and productivity; moves to available or planned hyper-spectral aircraft instruments; briefly describes synthetic aperture radar applications for waves and wind, and closes with a discussion of passive microwave measurements of salinity. Readers are directed to the Further Reading section if they desire additional information on individual topics.

Active Systems

Airborne Laser Fluorosensing

The concentrations of certain waterborne constituents, such as chl-a, can be measured from their fluorescence, a relationship that is exploited in shipboard sensors such as standard fluorometers and flow cytometers that are discussed elsewhere in this encyclopedia. NASA first demonstrated the measurement of laser-induced chl-a fluorescence from a low-flying aircraft in the mid-1970s. Airborne laser fluorosensors were developed shortly thereafter in the USA, Canada, Germany, Italy, and Russia, and used for measuring laser-induced fluorescence of a number of marine constituents in addition to chl-a. Oceanic constituents amenable to laser fluorosensing include phycoerythrin (photosynthetic pigment in some phytoplankton taxa), chromophoric dissolved organic matter (CDOM), and oil films. Airborne laser fluorosensors have also been used to follow dyes such as fluorescein and rhodamine that are introduced into water masses to trace their movement.

The NASA Airborne Oceanographic Lidar (AOL) is the most advanced airborne laser fluorosensor. The transmitter portion features a dichroic optical device to spatially separate the temporally concurrent 355 and 532 nm pulsed-laser radiation, followed by individual steering mirrors to direct the separated beams to respective oceanic targets separated by ~ 1 m when flown at the AOL's nominal 150 m operational altitude. The receiver focal plane containing both laser-illuminated targets is focused onto the input slits of the monochromator. The monochromator output focal planes are viewed by custom-made optical fibers that transport signal photons from the focal planes to the photo-cathode of each photo-multiplier module (PMM) where the conversion from photons to electrons takes place with a substantial gain. Time-resolved waveforms are collected in channels centered at 404 nm (water Raman) and 450 nm (CDOM) from 355 nm laser excitation, and at 560 nm and 590 nm (phycoerythrin), 650 (water Raman), and 685 nm (chl-a) from

the 532 nm laser excitation. The water Raman from the respective lasers is the red-shifted emission from the OH^- bonds of water molecules resulting from radiation with the laser pulse. The strength of the water Raman signal is directly proportional to the number of OH^- molecules accessed by the laser pulse. Thus, the water Raman signal is used to normalize the fluorescence signals to correct for variations in water attenuation properties in the surface layer of the ocean. The AOL is described in more detail on http://lidar.wff.nasa.gov.

The AOL has supported major oceanographic studies throughout the 1980s and 1990s, extending the usefulness of shipboard measurements over wide areas to permit improved interpretation of the ship-derived results. Examples of data from the AOL show horizontal structure of laser-induced fluorescence converted to chl-a concentration (**Figure 1**). Prominent oceanographic expeditions that have benefited from aircraft coverage with the AOL include the North Atlantic Bloom Experiment (NABE) of the Joint Global Ocean Flux Study (JGOFS), and the Iron Enrichment Experiment (IRONEX) of the Equatorial Pacific near the Galapagos Islands. This system has been flown on NASA P-3B aircraft in open-ocean missions that often exceeded 6 h in duration and collected hundreds of thousands of spectra. Each 'experiment' is able to generate both active and passive data in 'pairs' that are used for determining ocean color and recovering chl-a and other constituents, and that are also useful in the development of algorithms for measuring these constituents from oceanic radiance spectra.

Airborne Lidar Coastal Mapping

The use of airborne lidar (light detection and ranging) sensors for meeting coastal mapping

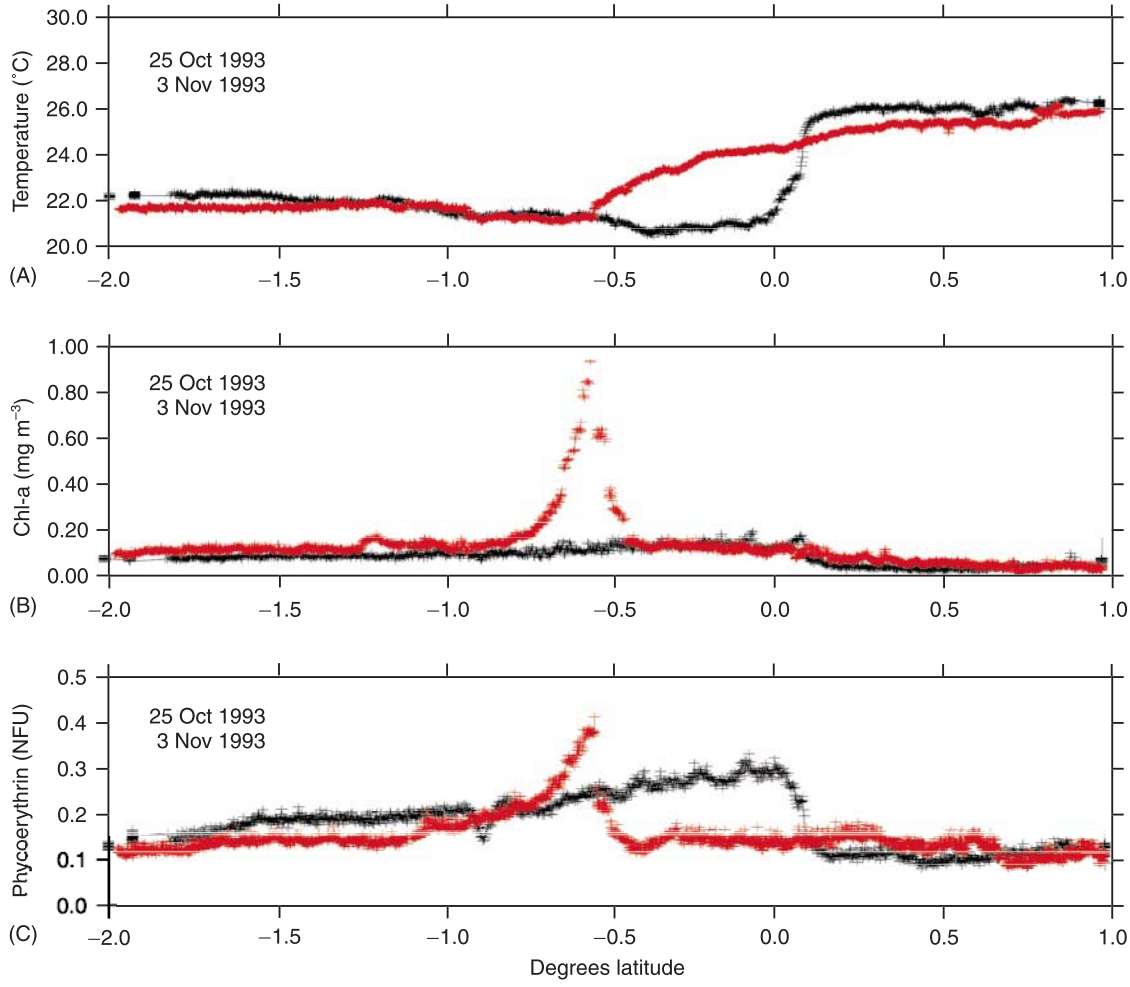

Figure 1 Cross-section profiles flown across a large oceanic front west of the Galapagos Islands on 25 October and 3 November 1993. (A) A dramatic horizontal displacement of the front as measured with an infrared radiometer; (B) and (C) show corresponding changes in laser-induced fluorescence of chl-a and phycoerythrin. This flight was made as part of the original IRONEX investigation in late 1993. NFU, normalized fluorescence units.

requirements is a relatively new and promising application of laser-ranging technology. These applications include high-density surveying of coastline and beach morphology and shallow water bathymetry. The capability to measure distance accurately with lidar sensors has been available since the early 1970s, but their application to airborne surveying of terrestrial features was seriously hampered by the lack of knowledge of the position of the aircraft from which the measurement was made. The implementation of the Department of Defense GPS constellation of satellites in the late 1980s, coupled with the development of GPS receiver technology, has resulted in the capability to provide the position of a GPS antenna located on an aircraft fuselage in flight to an accuracy approaching 5 cm using kinematic differential methodology. These methods involve the use of a fixed receiver (generally located at the staging airport) and a mobile receiver that is fixed to the aircraft fuselage. The distance between mobile and fixed receivers, referred to as the baseline, is typically on the order of tens of kilometers, and can be extended to hundreds of kilometers by using dual frequency survey grade GPS receivers aided by tracking the phase code of the carrier from each frequency.

Modern airborne lidars are capable of acquiring 5000 or more discrete range measurements per second. Aircraft attitude and heading information are used along with the GPS-determined platform position to locate the position of the laser pulse on the Earth's surface to a vertical accuracy approaching 10 cm with some highly accurate systems and < 30 cm for most of these sensors. The horizontal accuracy is generally 50–100 cm. Depending on the pulse repetition rate of the laser transmitter, the off-nadir pointing angle, and the speed of the aircraft platform, the density of survey points can exceed one sample per square meter.

NASA's Airborne Topographic Mapper (ATM) is an example of a topographic mapping lidar used for coastal surveying applications. An example of data from ATM shows shoreline features off the east coast of the USA (**Figure 2**). ATM was originally developed to measure changes in the elevation of Arctic ice sheets in response to global warming. The sensor was applied to measurements of changes in coastal morphology beginning in 1995. Presently, baseline topographic surveys exist for most of the Atlantic and Gulf coasts between central Maine and Texas and for large sections of the Pacific coast. Affected sections of coastline are re-occupied following major coastal storms, such as hurricanes and 'Nor'easters', to determine the extent of erosion and depositional patterns resulting from the storms. Additional details on the ATM and some results of investigations on coastal morphology can be found on websites (http://lidar.wff.nasa.gov and http://aol.wff.nasa.gov/aoltm/projects/beachmap/98results/).

Other airborne lidar systems have been used to survey coastal morphology, including Optec lidar systems by Florida State University and the University of Texas at Austin. Beyond these airborne lidar sensors, there are considerably more instruments with this capability that are currently in use in the commercial sector for surveying metropolitan areas, flood plains, and for other terrestrial applications. At the last count (early 2000) there were approximately 60 airborne lidars in operation worldwide, with most engaged in a variety of survey applications generally outside the field of coastal mapping.

Pump and Probe Fluorometry

Several sections in this chapter describe recoveries of phytoplankton biomass as chl-a by active and passive measurements. Another recent accomplishment is an active, airborne laser measurement intended to aid in remote detection of photosynthetic performance, an important ingredient of primary productivity computations. Fluorometric techniques, such as fast repetition rate (FRR) fluorometry (explained in another article of this encyclopedia), have provided an alternative approach to ^{14}C assimilation and O_2 evolution in the measurement of primary productivity. This technology has matured with the commercial availability of FRR instruments that can give vertical profiles or operate in a continuous mode while underway. There have been several attempts to develop airborne lidar instruments to determine phytoplankton photosynthetic characteristics from aircraft in the past decade. NASA scientists have deployed a pump and probe fluorometer from aircraft, wherein the AOL laser (described above) acts as the pump and a second laser with variable power options and rapid pulsing capabilities (10 ns) functions as the probe.

Passive Systems

Multichannel Ocean Color Sensor (MOCS)

Passive ocean color measurements using visible radiometers to measure reflected natural sunlight from the ocean have been made with a number of instruments in the past two decades. These instruments include the Multichannel Ocean Color Sensor (MOCS) that was flown in studies of Nantucket Shoals in the early 1980s, the passive sensors of the AOL suite that have been used in many locations around the world, and more recently, simple

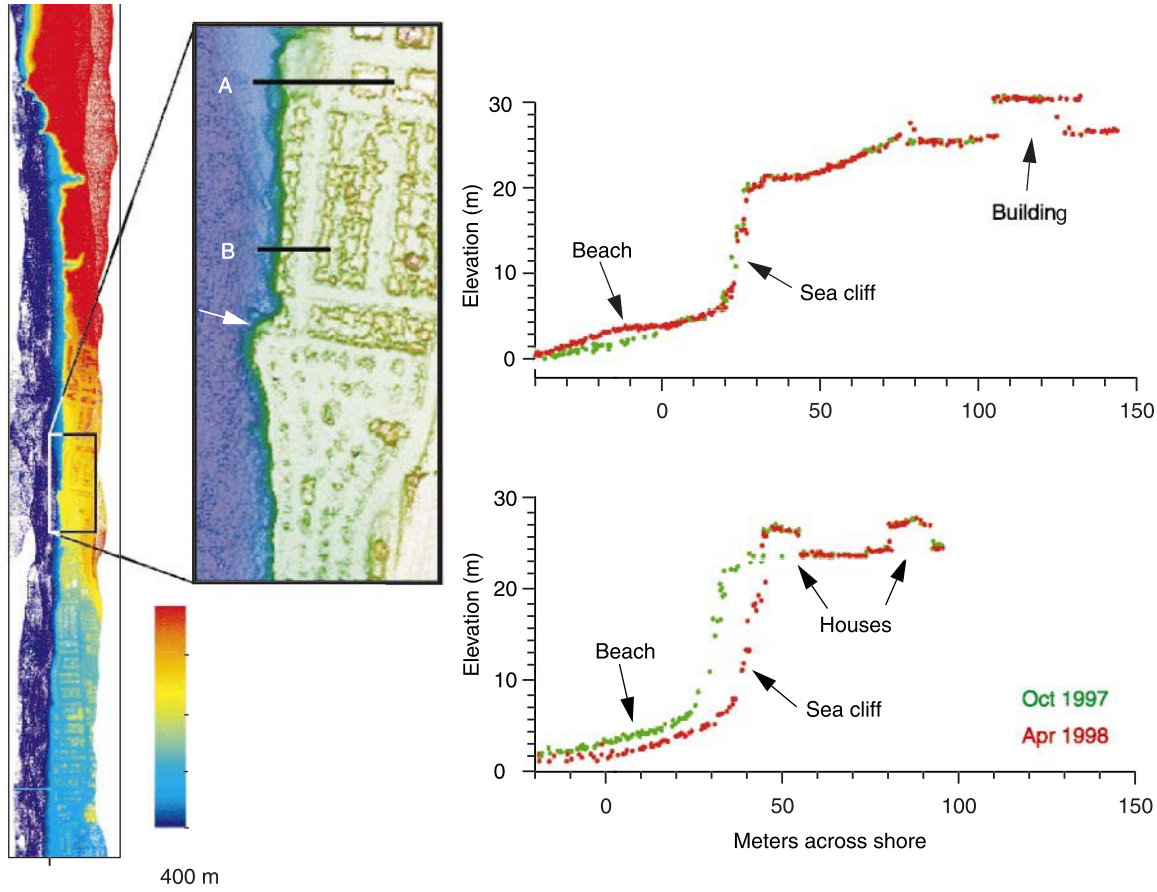

Figure 2 (Left) Map of coastal topography around Pacifica, CA, USA, derived from lidar data obtained in April 1998, after a winter of severe storms associated with El Niño. Map insert shows the Esplanade Drive area of Pacifica rendered from lidar data gridded at 2 m resolution and colored according to elevation. (Right) Cross-sections derived from lidar data of October 1997 and April 1998 at locations marked in the map inset. The profiles in (A) show a stable cliff and accreting beach, whereas about 200 m to the south the profiles in (B) show erosion of the sea cliff and adjacent beach resulting in undermining of houses. Each profile shows individual laser spot elevations that fall within a 2 m wide strip oriented approximately normal to shoreline. (Reproduced with permission from Sallenger *et al.*, 1999.)

radiometers that have been deployed on light aircraft in regional studies of Chesapeake Bay (see below). MOCS was one of the earliest ocean color sensors used on aircraft. It provided mesoscale data on shelf and slope chl-a in conjunction with shipboard studies of physical structure, nutrient inputs, and phytoplankton primary productivity.

Ocean Data Acquisition System (ODAS) and SeaWiFS Aircraft Simulator (SAS)

Few aircraft studies have obtained long time-series sufficient to quantify variability and detect secular trends. An example is ocean color measurements made from light aircraft in the Chesapeake Bay region for over a decade, providing data on chl-a and SST from >250 flights. Aircraft over-flights of the Bay using the Ocean Data Acquisition System (ODAS) developed at NASA's Goddard Space Flight Center commenced in 1989. ODAS was a nadir-viewing, line-of-flight, three-band radiometer with spectral coverage in the blue-green region of the visible spectrum (460–520 nm), a narrow 1.5° field-of-view, and a 10 Hz sampling rate. The ODAS instrument package included an IR temperature sensor (PRT-5, Pyrometrics, Inc.) for measuring SST. The system was flown for $\sim$7 years over Chesapeake Bay on a regular set of tracks to determine chl-a and SST. Over 150 flights were made with ODAS between 1989 and 1996, coordinated with *in situ* observations from a multi-jurisdictional monitoring program and other cruises of opportunity.

ODAS was flown together with the SeaWiFS Aircraft Simulator (SAS II, III, Satlantic, Inc., Halifax, Canada) beginning in 1995 and was retired soon thereafter and replaced with the SAS units. SAS III is

a multi-spectral (13-band, 380–865 nm), line-of-flight, nadir viewing, 10 Hz, passive radiometer with a 3.5° field-of-view that has the same wavebands as the SeaWiFS satellite instrument, and several additional bands in the visible, near IR, and UV. The SAS systems include an IR temperature sensor (Heimann Instruments, Inc.). Chl-a estimates are obtained using a curvature algorithm applied to water-leaving radiances at wavebands in the blue-green portion of the visible spectrum with validation from concurrent shipboard measurements. Flights are conducted at ~ 50–$60\,m\,s^{-1}$ (100–120 knots), giving an along-track profile with a resolution of 5–6 m averaged to 50 m in processing, and interpolated to $1\,km^2$ for visualization. Imagery derived from ODAS and SAS flights is available on a web site of the NOAA Chesapeake Bay Office for the main stem of the Bay (http://noaa.chesapeakebay.net), and for two contrasting tributaries, the Choptank and Patuxent Rivers on a web site of the Coastal Intensive Sites Network (CISNet) (http://www.cisnet-choptank.org).

Data from ODAS and SAS have provided detailed information on the timing, position, and magnitude of blooms in Chesapeake Bay, particularly the spring diatom bloom that dominates the annual phytoplankton cycle. This April–May peak of chl-a represents the largest accumulation of phytoplankton biomass in the Bay and is a proximal indicator of over-enrichment by nutrients. Data from SeaWiFS for spring 2000 show the coast-wide chl-a distribution for context, while SAS III data illustrate the high-resolution chl-a maps that are obtained regionally (**Figure 3**). A well-developed spring bloom corresponding to a year of relatively high freshwater flow from the Susquehanna River, the main tributary feeding the estuary, is apparent in the main stem Bay chl-a distribution. Estimates of primary productivity are now being derived from shipboard observations of key variables combined with high-resolution aircraft measurements of chl-a and SST for the Bay.

Hyper-spectral Systems

Airborne Visible/Infrared Imaging Spectrometer (AVIRIS)

The Airborne Visible/Infrared Imaging Spectrometer (AVIRIS) was originally designed in the late 1980s by NASA at the Jet Propulsion Laboratory (JPL) to collect data of high spectral and spatial resolution, anticipating a space-based high-resolution imaging spectrometer (HIRIS) that was planned for launch in the mid-1990s.

Because the sensor was designed to provide data similar to satellite data, flight specifications called for both high altitude and high speed. AVIRIS flies almost exclusively on a NASA ER-2 research aircraft at an altitude of 20 km and an airspeed of $732\,km\,h^{-1}$. At this altitude and a 30° field of view, the swath width is almost 11 km. The instantaneous field of view is 1 mrad, which creates individual pixels at a resolution of $20\,m^2$. The sensor samples in a whisk-broom fashion, so a mirror scans back and forth, perpendicular to the line-of-flight, at a rate of 12 times per second to provide continuous spatial coverage. Each pixel is then sent to four separate spectrometers by a fiber optic cable. The spectrometers are arranged so that they each cover a part of the spectrum from 0.40 to 2.4 μm, providing continuous spectral coverage at 10 nm intervals over the entire spectrum from visible to near IR. Data are recorded to tape cassettes for storage until rectification, atmospheric correction, and processing at JPL. A typical AVIRIS 'scene' is a 40 min flight line. At ER-2 flight parameters, this creates an image roughly 500 km long and 11 km wide. Data are encoded at 12-bits for a high degree of discrimination. The physical dimensions of AVIRIS are quite large, 84 cm wide × 160 cm long × 117 cm tall at a weight of 720 pounds.

Data collected with AVIRIS have been used for terrestrial, marine, and atmospheric applications. Accomplishments of AVIRIS include separation of the chl-a signature from bottom reflectance for clear lake waters of Lake Tahoe and turbid waters near Tampa Bay, interpretation of spectral signals from resuspended sediment and dissolved organic materials in W. Florida, and of suspended sediment and kelp beds in S. California. Recent efforts have focused on improving atmospheric correction procedures for both AVIRIS and satellite data, providing inputs for bio-optical models which determine inherent optical properties (IOPs) from reflectance, algorithm development, and sporadic attempts at water quality monitoring (e.g., chl-a, suspended sediment, diffuse attenuation coefficient, k_d). AVIRIS data have recently been used as an input variable to a neural network model developed to estimate water depth. The model was able to separate the contributions of different components to the total water-leaving radiance and to provide relatively accurate estimates of depth (rms error = 0.48 m).

Compact Airborne Spectrographic Imager (CASI)

The Compact Airborne Spectrographic Imager (CASI) is a relatively small, lightweight hyper-spectral sensor that has been used on a variety of light

aircraft. CASI was developed by Itres Research Ltd (Alberta, Canada) in 1988 and was designed for a variety of remote sensing applications in forestry, agriculture, land-use planning, and aquatic monitoring. By allowing user-defined configurations, the 12-bit, push-broom-type sensor (333 scan lines per second) using a charge-coupled detector (CCD) can be adapted to maximize either spatial (37.8° across track field of view, 0.077° along-track, 512 pixels – pixel size varies with altitude) or spectral

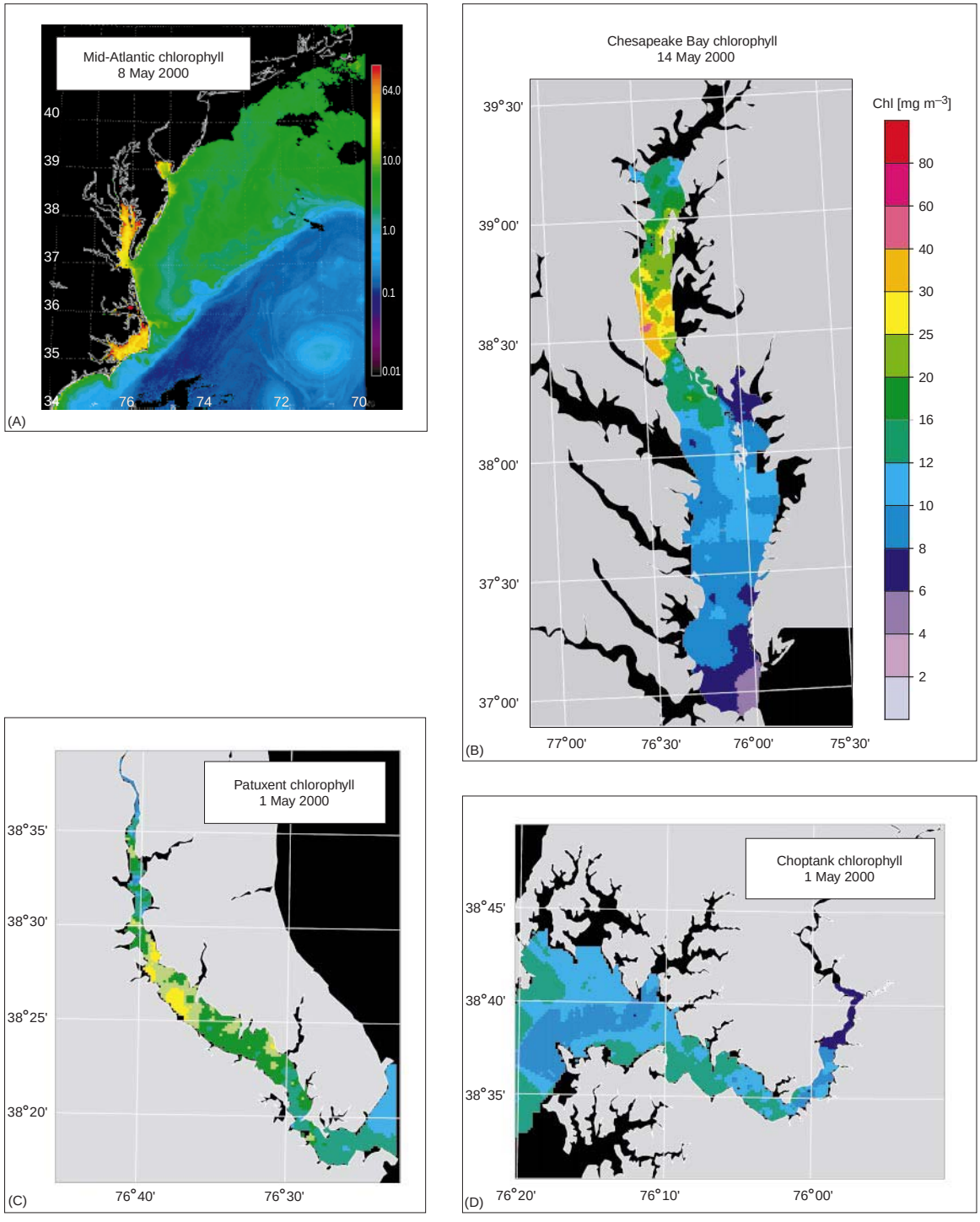

Figure 3 Spring chl-a (mg m^{-3}) in: (A) the mid-Atlantic region from SeaWiFS; (B) Chesapeake Bay; (C) Patuxent R; (D) Choptank R from SAS III.

resolution (288 bands at 1.9 nm intervals between 400 and 1000 nm). Experiments have been conducted using CASI to determine bottom type, benthic cover, submerged aquatic vegetation, marsh type, and in-water constituents such as suspended sediments, chl-a, and other algal pigments.

Portable Hyper-spectral Imager for Low-Light Spectroscopy (PHILLS)

The Portable Hyper-spectral Imager for Low-Light Spectroscopy (PHILLS) has been constructed by the US Navy (Naval Research Laboratory) for imaging the coastal ocean. PHILLS uses a backside-illuminated CCD for high sensitivity, and an all-reflective spectrograph with a convex grating in an Offner configuration to produce a distortion-free image. The instrument benefits from improvements in large-format detector arrays that have enabled increased spectral resolution and higher signal-to-noise ratios for imaging spectrographs, extending the use of this technology in low-albedo coastal waters. The ocean PHILLS operates in a push-broom scanned mode whereby cross-track ground pixels are imaged with a camera lens onto the entrance slit of the spectrometer, and new lines of the along-track ground pixels are attained by aircraft motion. The Navy's interest in hyper-spectral imagers for coastal applications centers on the development of methods for determining shallow water bathymetry, topography, bottom type composition, underwater hazards, and visibility. PHILLS precedes a planned hyper-spectral satellite instrument, the Coastal Ocean Imaging Spectrometer (COIS) that is planned to launch on the Naval Earth Map Observer (NEMO) spacecraft.

Radar Altimetry

Ocean applications of airborne radar altimetry systems include several sensors that retrieve information on wave properties. Two examples are the Radar Ocean Wave Spectrometer (ROWS), and the Scanning Radar Altimeter (SRA), systems designed to measure long-wave directional spectra and near-surface wind speed. ROWS is a K_u-band system developed at NASA's Goddard Space Flight Center in support of present and future satellite radar missions. Data obtained from ROWS in a spectrometer mode are used to derive two-dimensional ocean spectral wave estimates and directional radar backscatter. Data from the pulse-limited altimeter mode radar yield estimates of significant wave height and surface wind speed.

Synthetic Aperture Radar (SAR)

Synthetic Aperture Radar (SAR) systems emit microwave radiation in several bands and collect the reflected radiation to gain information about sea surface conditions. Synthetic aperture is a technique that is used to synthesize a long antenna by combining signals, or echoes, received by the radar as it moves along a flight track. Aperture refers to the opening that is used to collect reflected energy and form an image. The analogous feature of a camera to the aperture would be the shutter opening. A synthetic aperture is constructed by moving a real aperture or antenna through a series of positions along a flight track.

NASA's Jet Propulsion Laboratory and Ames Research Center have operated the Airborne SAR (AIRSAR) on a DC-8 since the late 1980s. The radar of AIRSAR illuminates the ocean at three microwave wavelengths: C-band (6 cm), L-band (24 cm), and P-band (68 cm). Brightness of the ocean (the amount of energy reflected back to the antenna) depends on the roughness of the surface at the length scale of the microwave (Bragg scattering). The primary source of roughness, and hence brightness, at the wavelengths used is capillary waves associated with wind. Oceanographic applications derive from the responsiveness of capillary wave amplitude to factors that affect surface tension, such as swell, atmospheric stability, and the presence of biological films. For example, the backscatter characteristics of the ocean are affected by surface oil and slicks can be observed in SAR imagery as a decrease of radar backscatter; SAR imagery appears dark in an area affected by an oil spill, surface slick, or biofilm, as compared with areas without these constituents.

Microwave Salinometers

Passive microwave radiometry (L-band) has been tested for the recovery of SSS from aircraft, and it may be possible to make these measurements from space. Salinity affects the natural emission of EM radiation from the ocean, and the microwave signature can be used to quantify SSS. Two examples of aircraft instruments that have been used to measure SSS in the coastal ocean are the Scanning Low-Frequency Microwave Radiometer (SLFMR), and the Electronically Thinned Array Radiometer (ESTAR).

SLFMR was used recently in the estuarine plume of Chesapeake Bay on the east coast of the USA to follow the buoyant outflow that dominates the near-shore density structure and constitutes an im-

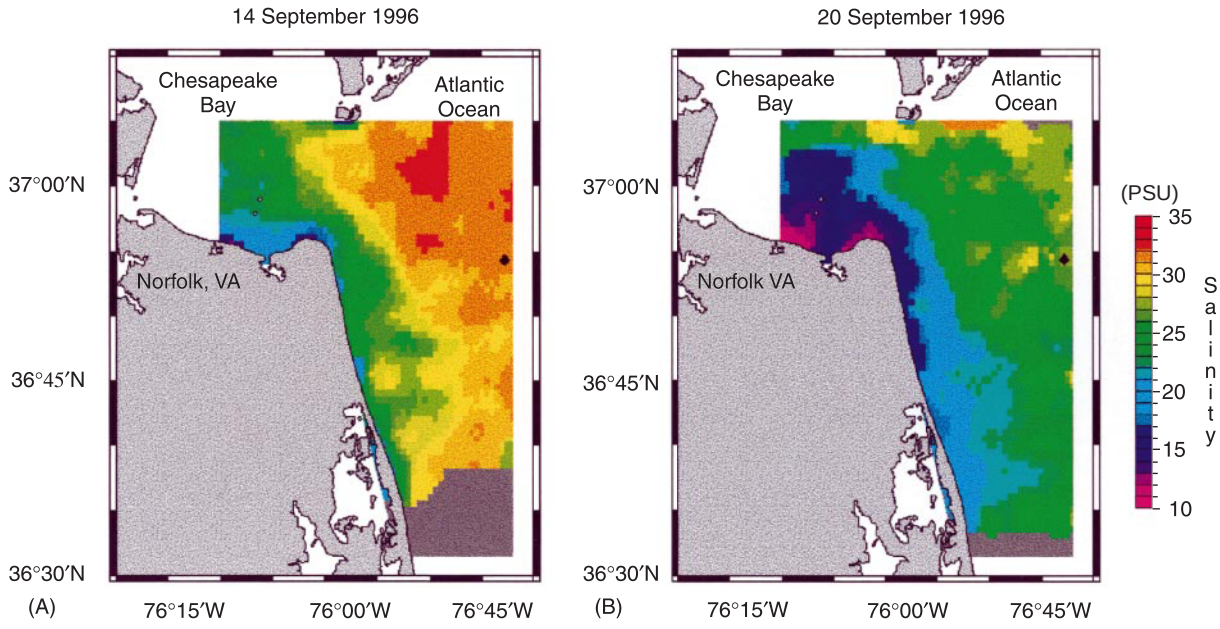

Figure 4 Sea surface salinity from an airborne microwave salinity instrument for (A) 14 September 1996; (B) 20 September 1996. Images reveal strong onshore-offshore gradients in salinity from the mouth of Chesapeake Bay to the plume and shelf, and the effect of high rainfall and freshwater input on the salinity distribution over a 1-week interval. (Adapted with permission from Miller *et al.*, 1998.)

portant tracer of water mass movement. SLFMR is able to recover SSS at an accuracy of about 1 PSU (**Figure 4**). This resolution is too coarse for the open ocean, but is quite suitable for coastal applications where significant gradients occur in regions influenced by freshwater inputs. SLFMR has a bandwidth of 25 MHz, a frequency of 1.413 GHz, and a single antenna with a beam width of approximately 16° and six across-track positions at $\pm 6°$, $\pm 22°$ and $\pm 39°$. Tests of SLFMR off the Chesapeake Bay demonstrated its effectiveness as a 'salinity mapper' by characterizing the trajectory of the Bay plume from surveys using light aircraft in joint operations with ships. Flights were conducted at an altitude of 2.6 km, giving a resolution of about 1 km. The accuracy of SSS in this example is ~ 0.5 PSU.

ESTAR is an aircraft instrument that is the prototype of a proposed space instrument for measuring SSS. This instrument relies on an interferometric technique termed 'aperture synthesis' in the across-track dimension that can reduce the size of the antenna aperture needed to monitor SSS from space. It has been described as a 'hybrid of a real and a synthetic aperture radiometer.' Aircraft surveys of SSS using ESTAR in the coastal current off Maryland and Delaware showed good agreement with thermosalinograph measurements from ships in the range of 29–31 PSU.

See also

Beaches, Physical Processes Affecting. Bio-optical Models. Fluorometry for Biological Sensing. Inherent Optical Properties and Irradiance. IR Radiometers. Iron Fertilization. Ocean Color from Satellites. Optical Particle Characterization. Phytoplankton Blooms. Primary Production Distribution. River Inputs. Satellite Measurements of Salinity. Satellite Oceanography, History and Introductory Concepts. Satellite Remote Sensing of Sea Surface Temperatures. Satellite Remote Sensing SAR. Upper Ocean Time and Space Variability.

Further Reading

Blume H-JC, Kendall BM and Fedors JC (1978) Measurement of ocean temperature and salinity via microwave radiometry. *Boundary Layer Meteorology* 13: 295–308.

Campbell JW and Esaias WE (1985) Spatial patterns in temperature and chlorophyll on Nantucket Shoals from airborne remote sensing data, May 7–9, 1981. *Journal of Marine Research* 43:139–161.

Harding LW Jr, Itsweire EC and Esaias WE (1994) Estimates of phytoplankton biomass in the Chesapeake Bay from aircraft remote sensing of chlorophyll concentrations, 1989–92. *Remote Sensing Environment* 49: 41–56.

Le Vine DM, Zaitzeff JB, D'Sa EJ *et al.* (2000) Sea surface salinity: toward an operational remote-sensing system. In: Halpern D (ed.) *Satellites, Oceanography and Society*, pp. 321–335. Elsevier Science.

Miller JL, Goodberlet MA and Zaitzeff JB (1998) Airborne salinity mapper makes debut in coastal zone. *EOS Transactions of the American Geophysical Union* 79: 173–177.

Sallenger AH Jr, Krabill W, Brock J *et al.* (1999) *EOS Transactions of the American Geophysical Union* 80: 89–93.

Sandidge JC and Holyer RJ (1998) Coastal bathymetry from hyper-spectral observations of water radiance. *Remote Sensing Environment* 65: 341–352.

AIR–SEA GAS EXCHANGE

B. Jähne, University of Heidelberg, Heidelberg, Germany

doi:10.1006/rwos.2001.0060

Introduction

The exchange of inert and sparingly soluble gases including carbon dioxide, methane, and oxygen between the atmosphere and oceans is controlled by a thin 20–200 μm thick boundary layer at the top of the ocean. The hydrodynamics in this layer are significantly different from boundary layers at rigid walls since the orbital motion of the waves is of the same order as the velocities in the viscous boundary layer. Laboratory and field measurements show that wind waves and surfactants significantly influence the gas transfer process. Because of limited experimental techniques, the details of the mechanisms and the structure of the turbulence in the boundary layer at a wavy water surface are still not known. A number of new imaging techniques are described that give direct insight into the transfer processes and promise to trigger substantial theoretical progress in the near future.

Theory

Mass Boundary Layers

The transfer of gases and volatile chemical species between the atmosphere and oceans is driven by a concentration difference and the transport by molecular and turbulent motion. Both types of transport processes can be characterized by diffusion coefficients, denoted by D and K_c, respectively. The resulting flux density j_c is proportional to the diffusion coefficient and the concentration gradient. Thus

$$j_c = (D + K_c(z))\nabla c \qquad [1]$$

where z is the vertical distance from the water surface. In a stationary homogeneous case and without sinks and sources by chemical reactions the flux density j is in vertical direction and constant. Then integration of eqn [1] yields vertical concentration profiles

$$C(z_r) - C(0) = j_c \int_0^{z_r} \frac{1}{D + K_c(z)} \mathrm{d}z \qquad [2]$$

The molecular diffusion coefficient is proportional to the velocity of the molecules and the free length between collisions. The same concept can be applied to turbulent diffusion coefficients. Far away from the interface, the free length (called mixing length) is set proportional to the distance from the interface and the turbulent diffusion coefficient K_c for mass transfer is

$$K_c = \frac{\kappa}{Sc_t} u_\star z \qquad [3]$$

where $\kappa = 0.41$ is the von Kármán constant, $u_\star$, the friction velocity, a measure for the velocity fluctuations in a turbulent flow, and $Sc_t = K_m/K_c$ the turbulent Schmidt number. Closer to the interface, the turbulent diffusion coefficients are decreasing even faster. Once at critical length scale l is reached, the Reynolds number $R_e = u_\star l/\nu$ (ν is the kinematic viscosity, the molecular diffusion coefficient for momentum) becomes small enough so that turbulent motion is attenuated by viscosity. The degree of attenuation depends on the properties of the interface. At a smooth solid wall, $K_c \propto z^3$, at a free water interface it could be in the range between $K_c \propto z^3$ and $K_c \propto z^2$ depending on surface conditions.

In any case, two boundary layers are formed. When the turbulent diffusivity becomes equal to the kinematic viscosity, the edge of the viscous boundary layer is reached. As the name implies, this layer is dominated by viscous dissipation and the velocity profile becomes linear because of a constant diffusivity. The edge of the mass boundary layer is reached when the turbulent diffusivity becomes equal to the molecular diffusivity. The relative thickness of both boundary layers depends on the dimensionless ratio $Sc = \nu/D$ (Schmidt number).